Journal of Ceramic Processing Research. Vol. 14, No. 3, pp. 371~375 (2013)

J O U R N A L O F
Ceramic Processing Research

Morphology control of Nb-doped SnO_2 nanofibres formed via electrospinning: From hollow nanofibres to dense nanofibres

Ha-Rim An and Hyo-Jin Ahn[a,*]

Department of Materials Science & Engineering, Seoul National University of Science and Technology, Seoul 139-743, Korea

Nb-doped SnO_2 nanofibres (NFs) with controlled morphologies were fabricated using an electrospinning method. In particular, structures ranging from hollow to dense were formed depending on the heating rate. To achieve this morphology control, relative mole ratios of the Nb precursor to the Sn precursor of 0.007, 0.021, and 0.035 were used, and the heating rate was 0.416, 0.625, 1.25, and 5 °C/min. The structural, compositional, and morphological properties of the obtained NFs were evaluated by means of X-ray diffraction (XRD), X-ray photoelectron spectroscopy (XPS), field-emission scanning electron microscopy (FE-SEM), and transmission electron microscopy (TEM). The succesful formation of hollow and dense Nb-doped SnO_2 NFs was found to be directly related to the use of a fast heating rate (5 °C/min) and a slow heating rate (0.416 °C/min), respectively. This relationship can be explained in terms of the diffusion of the ions decomposed from poly(vinypyrrolidone).

Key words: Electrospinning, Nb-doped SnO_2, Nanofibre, Hollow and dense structures.

Introduction

One-dimensional (1-D) nanostructures have recently received considerable interest in both academic and industrial fields because of their unique and fascinating properties and potential applications in sensors, transistors, photovoltaics, transparent electrodes, and photodetectors [1-5]. Previously, various synthetic methods such as electrospinning, template-assisted methods, the hydrothermal method, the laser-ablation method, and the thermal evaporation method have been developed to make 1-D nanostructures [1,6]. In particular, among the above-mentioned synthetic methods, the electrospinning method, in which nanofibres (NFs) are created from an electrically charged jet of polymer solution, is one of the most powerful methods for fabricating 1-D nanostructures. It possesses various advantages such as cost effectiveness, the ability to produce long and continuous NFs, good repeatability, easy control of the fibre dimensions, and a simple process [7]. Furthermore, various parameters influence the morphology of the NFs fabricated via electrospinning, namely, the applied voltage, the polymer solution, the collector, the distance between the needle tip and the collector, and the ambient conditions such as the humidity and temperature. Various NF morphologies of NFs such as porous, composite, core-shell, and hollow structures have been developed by manipulating the above-mentioned parameters [8-11]. Among the various NF morphologies, the hollow structures of SnO_2-based NFs, which are n-type semiconductors, have recently been of considerable interest for many potential applications including gas sensors, Li ion batteries, dye-sensitized solar cells (DSSCs), and photocatalysts. These hollow structures are particularly attractive because of their enhanced surface area compared to that of the usual dense NF structures [12-15]. For this reason, different strategies for fabricating hollow NFs for use in the above-mentioned applications have been developed. For example, Li *et al.* reported on the synthesis of hollow SnO_2 NFs for high-performance Li-ion batteries using large weight ratios of poly(vinylpyrrolidone) (PVP) and $SnCl_2$ in the precursor [13]. Gao *et al.* demonstrated how hollow SnO_2 NFs for high-performance DSSCs could be formed by manipulating the calcination temperature from 300 to 350 to 425 °C [14]. Wang *et al.* reported that hollow SnO_2 NFs can be formed by using homogeneous polymer-sol-double solvents because of the solvent evaporation and phase segregation [15]. However, among the various factors leading to the hollow structures of NFs, the different heating rates that can be used to produce hollow SnO_2-based NFs have not been studied yet.

In this study, SnO_2-based NFs with structures ranging from hollow to dense were fabricated by using an electrospinning technique in which different heating rates of 0.416, 0.625, 1.25, and 5 °C/min were used to control the morphology. Nb-doped SnO_2 was chosen as the material because it is a promising replacement for the Sn-doped In_2O_3 (ITO) used currently in transparent conductive electrodes (TCEs) thanks to its high conductivity ($\rho \sim 6.65 \times 10^{-3}\ \Omega$ cm) and high transmittance (~ 85%) [16].

*Corresponding author:
Tel : +82-2-970-6622
Fax: +82-2-973-6657
E-mail: hjahn@seoultech.ac.kr

Experimental Procedures

Nb-doped SnO_2 NFs with structures ranging from hollow to dense were synthesised using an electrospinning technique as follows. The tin chloride dehydrate ($SnCl_2 \cdot 2H_2O$, Aldrich, 99.9%) was dissolved in *N,N*-dimethylformamide (C_3H_7NO, Aldrich, 99%) for 1 h, and then niobium ethoxide ($Nb(OCH_2CH_3)_5$, Aldrich, 99.9%) was added. In order to fabricate Nb-doped SnO_2 NFs, relative mole ratios of the Nb precursor to the Sn precursor of 0.007, 0.021, 0.035, and 0.035 (referred herein to as samples A, B, C, and D) were used. After the niobium precursor had dissolved perfectly, PVP ($(C_6H_9NO)n$, $M_w = 1\ 300\ 000$ g/mol, Aldrich) was added to the mixture, which was then stirred for 1 h. The distance between the 23-gauge needle tip and the collector (aluminium foil) was fixed at ~20 cm. The applied voltage of the power supply was 18 kV, and the feeding rate was fixed at ~0.02 mL/h. The calcination temperature was fixed at 500 ºC, but heating rates of 0.416, 0.625, 1.25, and 5 ºC/min were used for sample D to find the effect of the heating rate on the morphology of the Nb-doped SnO_2 NFs. Finally, Nb-doped SnO_2 NFs with structures ranging from hollow to dense were obtained.

X-ray diffraction (XRD, Rigaku X-ray diffractometer equipped with Cu Kα radiation) was used to determine the crystalline structure of all the samples. X-ray photoelectron spectroscopy (XPS, ESCALAB 250 equipped with an Al Kα X-ray source) was used to analyze the chemical composition of all the samples. Field-emission scanning electron microscopy (FESEM, Hitachi S-4700) and transmission electron microscopy (TEM, JEOL-2100F operated at 200 kV) were used to characterize the structural and morphological properties of all the samples.

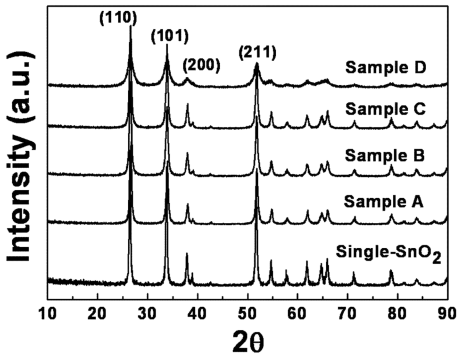

Fig. 1. Powder XRD data of single SnO_2, and of samples A, B, C, and D obtained after calcination at 500 ºC.

Results and Discussion

Fig. 1 shows XRD plots of single SnO_2 NFs, as well as those of samples A, B, C, and D after calcination at 500 ºC. XRD peaks were observed at 26.5 º, 33.8 º, 37.8 º, and 51.8 º for the single SnO_2 NFs, corresponding to the (110), (101), (200), and (211) planes, respectively. This is in good agreement with the peaks of cassiterite SnO_2 phases (JCPDS No. 77-0447), which have tetragonal rutile structures (space group $P4_2/mnm$ [136]). For samples A, B, C, and D, the characteristic diffraction peaks relative to the (110) planes occurred at slightly higher 2θ values because of the Nb doping. Since the ionic radius of Nb^{5+} (0.62 Å) is smaller than that of Sn^{4+} (0.69 Å), this peak shift can be explained using the Bragg equation,

$$\lambda = 2d \sin\theta \tag{1}$$

where λ is the X-ray wavelength, d is the lattice distance of the sample, and θ is the Bragg angle. Interestingly, sample D exhibits broader diffraction

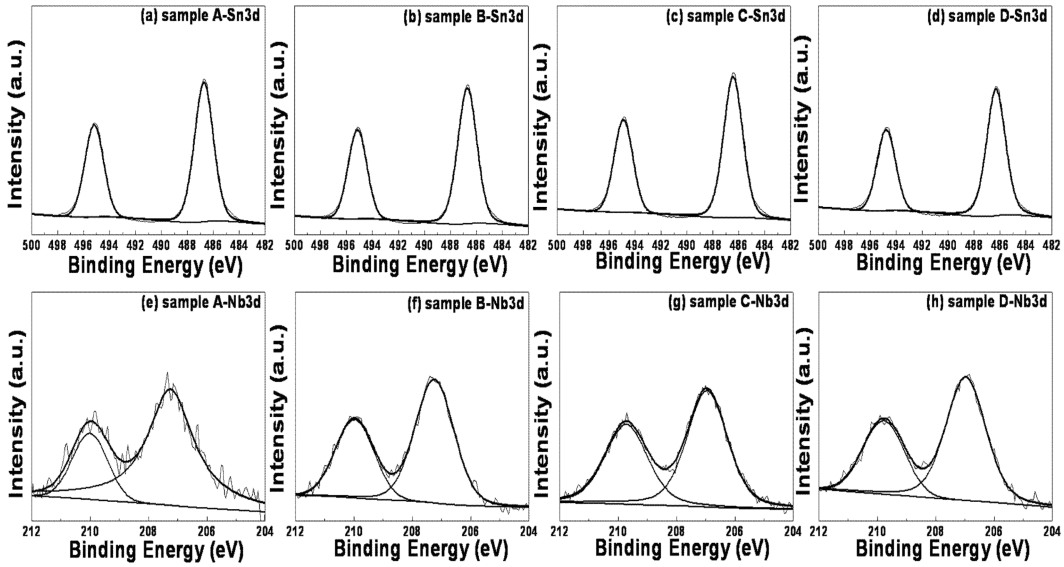

Fig. 2. XPS spectra of the Sn 3*d* and the Nb 3*d* core levels obtained from samples A, B, C, and D.

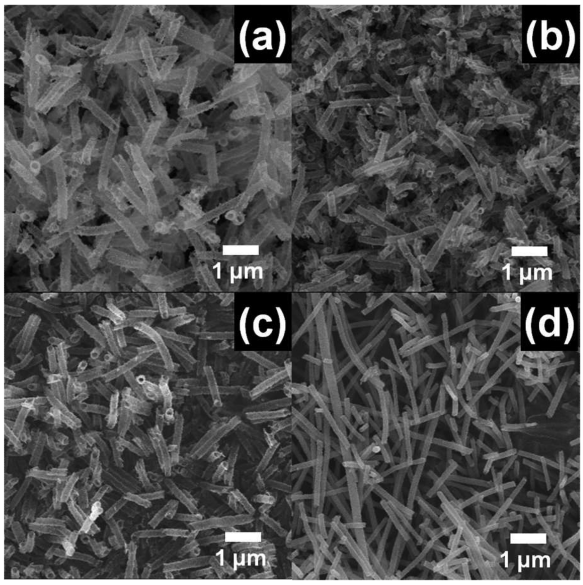

Fig. 3. FE-SEM images obtained from (a) sample A, (b) sample B, (c) sample C, and (d) sample D after calcination at 500 ºC.

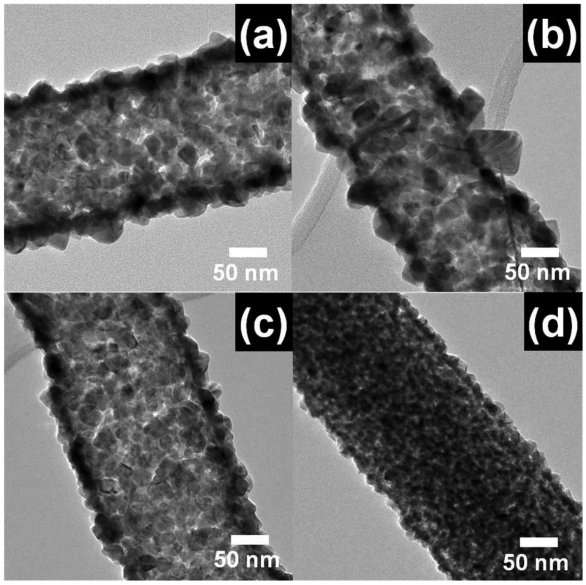

Fig. 4. TEM bright field images obtained from (a) sample A, (b) sample B, (c) sample, and (d) sample D after calcination at 500 ºC.

peaks than samples A, B, and C in terms of the full width at half-maximum (FWHM). This implies that the mean grain size of sample D is smaller than those of samples A, B, and C. This can be explained using the Scherrer equation [17],

$$D = 0.9\lambda/(B\cos\theta) \quad (2)$$

where D is the mean grain size, λ is the X-ray wavelength, B is the FWHM, and θ is the Bragg angle. Thus, the mean grain size (D) of sample D is in good agreement with the results obtained from the TEM results (see Fig. 4 for details of samples A, B, C, and D).

Fig. 2 shows the XPS spectra of the Sn 3*d* and Nb 3*d* core levels obtained from samples A, B, C, and D. The XPS peaks for the Sn $3d_{5/2}$ and $3d_{3/2}$ photoelectrons with area ratios of 1.5 are observed at ~486.7 and ~495.2 eV for sample A, ~486.7 and ~495.2 eV for sample B, ~486.4 and ~494.9 eV for sample C, and ~486.3 and ~494.8 eV for sample D. This implies that the chemical state of the Sn in the NFs is not Sn(II) but rather Sn(IV), which corresponds to the elemental Sn in SnO_2 [18]. In addition, the XPS peaks for the Nb $3d_{5/2}$ and $3d_{3/2}$ photoelectrons are observed at ~207.2 and ~209.9 eV for sample A, ~207.2 and ~209.8 eV for sample B, ~207.0 and ~209.8 eV for sample C, and ~207.0 and ~209.8 eV for sample D. This implies that the chemical state of the Nb in the NFs is not Nb (II) but rather Nb (V), which corresponds to the elemental Nb in Nb_2O_5 [18, 19]. Thus, the NFs consist of SnO_2 phases and Nb_2O_5 phases, and the successful formation of Nb-doped SnO_2 NFs is demonstrated by the XRD and XPS results.

Figs. 3(a-d) show the FE-SEM images of samples A, B, C, and D obtained after calcination at 500 ºC. In order to investigate the morphological changes of the samples, the heating rate was 5.00 ºC/min for samples A, B, and C and 0.41 ºC/min for sample D. The FESEM results in Fig. 3(a-c) show hollow Nb-doped SnO_2 NFs with diameters in the range of ~224 - ~293 nm, ~189 - ~218 nm, and ~180 - ~245 nm for samples A, B, and C, respectively. Furthermore, sample D (Fig. 3(d)) has dense Nb-doped SnO_2 NFs with diameters in the range of ~147 - ~241 nm. To further investigate the morphology of all the samples, we also carried out TEM examinations.

Figs. 4(a-d) show bright-field TEM images of samples A, B, C, and D. It is noted that samples A, B, and C exhibit a relatively dark, band-like contrast in the edge area and a relatively bright contrast in the core area, which indicates the successful formation of the hollow NFs. However, sample D has a uniform contrast over the entire area of the NFs, indicating the formation of the dense NFs. Furthermore, the mean grain sizes in the edge areas of the NFs are measured to be ~34 - ~72 nm for sample A, ~20 - ~59 nm for sample B, ~23 - ~40 nm for sample C, and ~10 - ~17 nm for sample D. Samples A, B, and C, which have hollow structures, have larger grains than the sample D, which has a dense structure, because of the parallel aggregation of ions near the edge area. One factor influencing the morphology of samples C and D is the heating rate. Therefore, to investigate the different mechanisms by which the dense and hollow structures form, the dependence of the morphology on the heating rate (ºC/min) of sample D was investigated as shown in Fig. 5. The mole ratio of the Nb precursor to the Sn precursor was 0.035 in sample D, and heating rates (ºC/min) of 0.416, 0.625, 1.25, and 5 ºC/min were used. It is found that faster heating rates led to better hollow structures

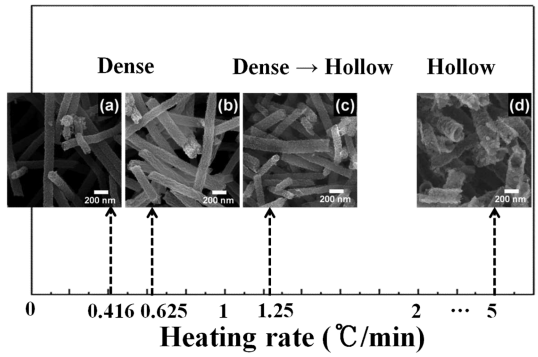

Fig. 5. dependence of heating rates (°C/min) of sample D; (a) 0.416, (b) 0.625, (c) 1.25, and (d) 5 °C/min during calcination at 500 °C.

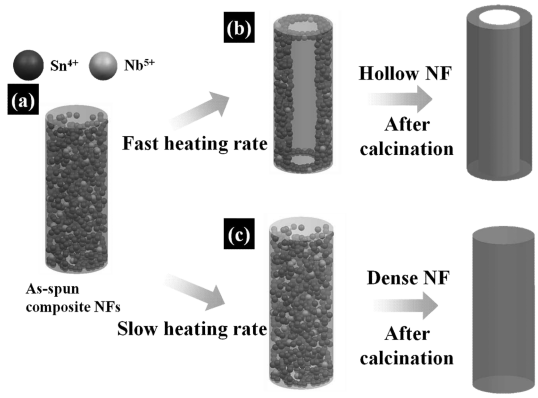

Fig. 6. A schematic diagram on the formation process of hollow and dense Nb-doped SnO_2 NFs depending on the heating rates.

of the Nb-doped SnO_2 NFs. In particular, the Nb-doped SnO_2 NFs had hollow structures for heating rates above 1.25 °C/min and dense structures for heating rates from 0.416 to 1.25 °C/min. The origin of this morphology change from hollow to dense structures can be explained by the schematic shown in Figs. 6(a-c). Fig. 6(a) shows the as-spun composite NFs consisting of the tin metal precursor in PVP and niobium metal precursor in PVP before calcination. The Sn ions and Nb ions are uniformly distributed in the as-spun NFs. Figs. 6(b) and 6(c) show a possible mechanism for the formation of hollow Nb-doped SnO_2 NFs involving the diffusion of ions decomposed from PVP [19]. When a fast heating rate is used (5 °C/min) for the calcinations at 500 °C, Sn ions and Nb ions decomposed from the PVP in the core areas of the NFs move toward the edge areas and encounter oxygen in the air, leading to the formation of hollow NFs, as shown in Fig. 6(b). Furthermore, the accumulation of Sn atoms and Nb atoms in the edge areas increases the grain size of the hollow NFs (see Figs. 4(a-c)). If the heating rate is too slow (0.416 °C/min), the ions cannot diffuse toward the edge area because of the slow decomposition reaction, leading to the formation of dense NFs. The mean grain size of these dense NFs is smaller than that of the hollow NFs owing to the uniform distribution of Sn atoms and Nb atoms in the NFs. In summary, we successfully demonstrated the morphology control of Nb-doped SnO_2 NFs with structures ranging from hollow to dense depending on the different heating rates.

Conclusions

Nb-doped SnO_2 NFs with structures ranging from hollow to dense were synthesised using an electrospinning method. The SEM, TEM, XRD, and XPS results demonstrated the morphological properties of the obtained Nb-doped SnO_2 NFs. The heating rate was found to have an important influence on the morphology of the samples. In particular, in order to control the morphology of the samples, heating rates of 0.416, 0.625, 1.25, and 5 °C/min were used for sample D. Hollow Nb-doped SnO_2 NFs are formed at fast heating rates in the range from 1.25 to 5 °C/min, and dense Nb-doped SnO_2 NFs are formed at slow heating rates in the range from 0.416 to 1.25 °C/min. The possible formation mechanisms for the hollow and dense Nb-doped SnO_2 NFs involved the different diffusion behaviours of the ions decomposed from PVP.

Acknowledgment

This work was supported by Grant No. 10041161 from the Ministry of Knowledge Economy (MKE) and Fundamental R & D Program for Core Technology of Materials funded by the Ministry of Knowledge Economy, Republic of Korea.

References

1. G. Shen, P.-C. Chen, K. Ryu and C. Zhou, J. Mater. Chem. 19 (2009) 828-839.
2. D. Chen, Z. Liu, B. Ling, X. Wang and G. Shen, Nanoscale 4 (2012) 3001-3012.
3. S.I. Noh, T.-Y. Seong and H.-J. Ahn, J. Ceram. Process Res. 13 (2012) 491-494.
4. H. Wu, L. Hu, M.W. Rowell, D. Kong, J.J. Cha, J.R. McDonough, J. Zhu, Y. Yang, M.D. McGehee and Y. Cui, Nano Lett. 10 (2010) 4242-4248.
5. T. Zhai, X. Fang, M. Liao, X. Xu, H. Zeng, B. Yoshio and D. Golberg, Sensors 9 (2009) 6504-6529.
6. S.I. Noh and H.-J. Ahn, J. Ceram. Process Res. 13 (2012) s1-s5.
7. S. Rmakrishna, K. Fujihara, W.-E. Teo, T.-C. Lim and Z. Ma, An Introduction to Electrospinning and Nanofibers, World Scientific Publishing Co. Ltd, Singapore, 2005.
8. J.T. McCann, M. Marquez and Y. Xia, J. Am. Chem. Soc. 128 (2006) 1436-1437.
9. G.-H. An and H.-J. Ahn, Ceram. Int. 38 (2012) 3197-3201.
10. G.-H. An and H.-J. Ahn, Solid State Sci. 14 (2012) 1050-1054.
11. J.T. McCann, D. Li and Y. Xia, J. Mater. Chem. 15 (2005) 735-738.
12. J.K. Choi, I.-S. Hwang, S.-J. Kim, J.-S. Park, S.-S. Park, U. Jeong, Y.C. Kang and J.-H. Lee, Sensor. Actuat. B-Chem. 150 (2010) 191-199.

13. L. Li, X. Yin, S. Liu, Y. Wang, L. Chen and T. Wang, Electrochem. Commun. 12 (2010) 1383-1386.
14. C. Gao, X. Li, B. Lu, L. Chen, Y. Wang, F. Teng, J. Wang, Z. Zhang, X. Pan and E. Xie, Nanoscale 4 (2012) 3475-3481.
15. P. Ren, H. Fan and X. Wang, Catal. Commun. 25 (2012) 32-35.
16. Y.J. Seo, G.W. Kim, C.H. Sung, M.S. Anwar, C.G. Lee and B.H. Koo, Curr. Appl. Phys. 11 (2011) S310-S313.
17. H.-J. Ahn, H.-C. Choi, K.-W. Park, S.-B. Kim and Y.-E. Sung, J. Phys. Chem. B 108 (2004) 9815-9820.
18. J.F. Moulder, W.F. Stickle, P.E. Sobol and K.D. Bomben, Handbook of X-ray Photoelectron Spectroscopy, Physical Electronics, Eden Pairie, MN, 1995.
19. M. Aufray, S. Menuel, Y. Fort, J. Eschbach, D. Rouxel and B. Vincent, J. Nanosci. Nanotechnol. 9 (2009) 4780-4785.